Am J Transl Res 2022;14(8):5441-5454
www.ajtr.org /ISSN:1943-8141/AJTR0142968

Original Article

LncRNA MIR4435-2HG promotes proliferation, migration, invasion and epithelial mesenchymal transition via targeting miR-22-3p/TMEM9B in breast cancer

Jing Ke[1], Quhui Wang[1], Wei Zhang[1], Sujie Ni[2], Haijun Mei[1]

Departments of [1]General Surgery, [2]Medical Oncology, Affiliated Hospital of Nantong University, Nantong 226001, Jiangsu Province, China

Received March 19, 2022; Accepted June 12, 2022; Epub August 15, 2022; Published August 30, 2022

Abstract: Objective: Breast cancer, as a malignancy with the highest incidence and mortality in women, seriously threatens women's life and health. Pieces of evidence have suggested that long non-coding RNAs (lncRNAs) possess important roles in regulating the occurrence and development of breast cancer. Methods: RT-qPCR was used to explore the expression levels of MIR4435-2HG, miR-22-3p and TMEM9B in breast cancer tissues and cell lines. Cell viability, proliferation, migration and invasion were assessed by CCK-8 assay, Colony formation assay, Wound healing assay and Transwell assay, respectively. The effect of MIR4435-2HG on EMT progress was explored by Immunofluorescence assay and Western blot. RNA pull-down analysis and Dual-luciferase reporter assay were performed to validate the interaction between MIR4435-2HG and miR-22-3p, as well as miR-22-3p and TMEM9B. Results: MIR4435-2HG was notably up-regulated in breast cancer tissues and cell lines. Additionally, down-regulation of MIR4435-2HG restrained the viability, proliferation, migration, invasion and EMT of breast cancer cells. MiR-22-3p expression was down-regulated in breast cancer tissues and cell lines, and negatively associated with MIR4435-2HG expression. Over-expression of miR-22-3p obviously inhibited the viability, proliferation, migration, invasion and EMT of breast cancer cell lines. Furthermore, TMEM9B was up-regulated in breast cancer tissues and cell lines and negatively associated with miR-22-3p expression. TMEM9B inhibition partially restored the effects of MIR4435-2HG/miR-22-3p on the viability, proliferation, migration, invasion and EMT of breast cancer cell lines. Conclusion: MIR4435-2HG plays a potential tumor-promoting role in the occurrence and development of breast cancer, possibly by regulating the miR-22-3p/TMEM9B axis.

Keywords: Breast cancer, LncRNA MIR4435-2HG, miR-22-3p, TMEM9B, target

Introduction

Breast cancer is a malignant tumor originating from breast epithelial tissues and is also the most common malignant disease in women [1]. Recent reports have shown that the incidence rate of breast cancer is increasing annually [2]. There are more than 1.3 million newly diagnosed cases of breast cancer in the world every year, and breast cancer accounts for 15% of newly diagnosed female tumors in China [3]. With the development of early detection, early diagnosis, early treatment, and prognosis monitoring of breast cancer, the overall mortality of breast cancer patients has decreased [4]. However, malignant proliferation, recurrence, metastasis and other factors may compensate these benefits. There are more than 45,000 deaths from breast cancer in the world every year [5]. The Chinese population accounts for 9.2% of the global deaths, making China the greatest contributor [6]. Therefore, breast cancer is still a serious threat to women's life and health in China. Further understanding the molecular mechanisms of the occurrence and development of breast cancer will be conducive to the targeted treatment of breast cancer [7, 8].

Long non-coding RNAs (LncRNAs) are a kind of non-coding RNAs with a length from 200 bp to 100 kbp. LncRNAs account for 4%-9% of the

transcripts in the mammalian genome and have attracted increasing interest [9]. With the rapid development of RNA sequencing, epigenome technology and computational prediction technology, an increasing number of lncRNAs have been discovered. Previous studies have shown that lncRNAs are abnormally expressed in breast cancer. Yang *et al*. identified more than 1300 abnormal lncRNAs in breast cancer by sequencing [10]. In addition, Shen *et al.* identified more than 1750 lncRNAs differentially expressed in triple-negative breast cancer [11]. These results suggested that abnormal expression of lncRNAs may play an important role in the carcinogenesis of breast cancer. Lv *et al*. found that the expression of lncRNAs in triple-negative breast cancer were different from those in non-triple negative breast cancer, so lncRNAs can be used as biomarkers for individual diagnosis, and may also be potential targets for evaluating individual therapeutic efficacy [12]. Moreover, lncRNA H19, SRA, LSINCT5 and UCA1 promoted the proliferation and/or metastasis of breast cancer. On the contrary, lncRNA GAS5 and XIST suppressed the proliferation and/or metastasis of breast cancer [13].

LncRNA MIR4435-2HG, known as AK001796 and LINC00978, is encoded on human chromosome 2q13 and has been regarded as a new oncogenic lncRNA in many types of cancers [14]. For example, a high level of MIR4435-2HG was detected in colorectal cancer tissues [15]. Increased level of MIR4435-2HG was significantly correlated with TNM stage and carcinoembryonic antigen level before treatment. High MIR4435-2HG expression can suggest a poorer progression-free survival and overall survival (OS) rate [15]. In addition, MIR4435-2HG was up-regulated in hepatocellular carcinoma tissues, and the expression of MIR4435-2HG was significantly affected by tumor size instead of tumor metastasis [16]. Additionally, MIR4435-2HG was over-expressed in ovarian cancer tissues and cells. MIR4435-2HG knockdown blocked the proliferation, invasion and migration but induced apoptosis of ovarian cancer cells via the miR-128-3p/CDK14 axis [17]. However, the exact function and corresponding mechanism of MIR4435-2HG in the occurrence and development of breast cancer have been rarely reported [17]. Therefore, the present study was designed to determine whether MIR4435-2HG exerted its functional role in the growth and metastasis of breast cancer, and to investigate its possible mechanisms.

Materials and methods

Clinical tissue collection

A total of 60 tissues, including 15 tissues in stage I-II, 15 tissues in stage III-IV, and 30 corresponding adjacent non-cancerous tissues were collected from the Affiliated Hospital of Nantong University. All patients in the study did not receive any chemotherapy and signed the written informed consent. Moreover, the experimental procedures were approved by the Ethics Committee of Affiliated Hospital of Nantong University (2021-L124). Patients' overall survival from the date of surgery to death or the end of follow-up was followed by telephone at a four-month interval for a total of 100 months.

Cell lines

Breast cancer cell lines, including Hs-578T, MCF-7, ZR-75-30 and HCC1937, and human breast epithelial cell line MCF-10A were obtained from the Chinese Academy of Science (Shanghai, China). Cells were routinely cultured in Dulbecco's Modified Eagle Medium (DMEM, KeyGEN, Nanjing, China) with 10% fetal bovine serum (FBS, Gibco, USA) and 1% penicillin-streptomycin (Sigma-Aldrich, USA) in a humidified atmosphere with 5% CO_2 at 37°C.

Cell transfection

Short hairpin RNA (sh)-MIR4435-2HG (5'-GGTCTGGTCGGTTTCCCATTT-3'), sh-TMEM9B (5'-GAAGCUCUGUCACAAUCAA-3'), miR-22-3p mimic (Sense: 5'-AAGCUGCCAGUUGAAGAACUGU-3', Antisense: 5'-AGUUCUUCAACUGGCAGCUUUU-3'), miR-22-3p inhibitor (5'-ACAGUUCUUCAACUGGCAGCUU-3') and corresponding negative control (NC) vectors were obtained from Gene Pharma Company (Shanghai, China). Lipofectamine 3000 (Invitrogen, USA) was performed for cell transfection based on the specification.

Cell counting kit-8 (CCK-8) assay

Transfected MCF-7 and ZR-75-30 cells (1×10^4 cells/well) were maintained in a 96-well plate

and cultured for different time periods (0, 24, 48 and 72 h, respectively). Then, cell viability was determined by a CCK-8 kit (Beyotime, Shanghai, China) according to the protocols of the manufacturer. The optical density was measured at 450 nm by using a microplate reader (BioTek Instruments Inc., Winooski, VT, USA).

Colony formation assay

Transfected MCF-7 and ZR-75-30 cells (1×10^3 cells/well) were seeded in a six-well plate. The media was replaced with a fresh culture medium every 2-3 days for 2 weeks. Subsequently, MCF-7 and ZR-75-30 cells were stained with 10% crystal violet for 30 min and observed with the use of a microscope (Olympus, Tokyo, Japan).

Wound healing assay

Transfected MCF-7 and ZR-75-30 cells (5×10^5 cells/well) were inoculated into a six-well plate. When the cells were 100% confluent, a wound was made on the surface of the cells using a 200 μL tip. After 0 and 48 h, MCF-7 and ZR-75-30 cells were observed under an inverted microscope (Tokyo, Japan), and the distance between the scratch was recorded.

Transwell migration and invasion assays

For migration and invasion assays, transfected MCF-7 and ZR-75-30 cells (1×10^6 cells/well) were seeded in the transwell chambers containing an 8 μm size porous membrane (Corning, NY, USA). The upper chamber was inserted without (for migration assay) or with matrigel (for invasion assay), while the lower chamber was added with 20% FBS. After 48 h of incubation at 37°C, the non-migrating or invading cells in the upper chamber were removed by cotton ball. The migrated or invaded cells in the upper chamber were stained with 0.1% crystal violet solution (Sangon Biotech, Shanghai, China) and counted under a microscope (Olympus, Tokyo, Japan).

RNA extraction and qRT-PCR analysis

RNA from clinical tissues and cell lines was extracted according to the instructions of the TRIzol reagent. The OD_{260}/OD_{280} of the RNA solution was also detected. The reverse transcription reaction was conducted according to the instructions of the cDNA synthesis kit, and the PCR reaction solution was configured according to the instructions of the Taq enzyme mixture. The PCR reaction conditions were: 50°C for 2 min, 95°C for 10 min (1 cycle), 95°C for 5 s, 65°C for 1 min, 75°C for 20 s (45 cycles); and 75°C for 5 min (1 cycle). Each real-time PCR was repeated 3 times. The primers were as follows: MIR4435-2HG forward, 5'-CGGAGCATGGAACTCGACA-3', and reverse, 5'-CAAGTC TCACACATCCGGG-3'. MiR-22-3p forward, 5'-AAGCTGCCAGTTGAAGAACTGTA-3', and reverse, 5'-GCTGTCAACGATACGCTACG-TAAC-3'. TMEM9B forward, 5'-AAAGTCCGCCA-TTTTGCCAC-3', and reverse, 5'-ATTCGGGGCT-CTGTAGTCCT-3'. U6 forward, 5'-CTCGCTTCGG-CAGCACA-3', and reverse, 5'-AACGCTTCACGA-ATTTGCGT-3'. β-actin forward, 5'-TCGTGGAA-GGACTCATGACC-3', and reverse, 5'-ATGATGT-TCTGGAGAGCCCC-3'. The fold change of gene expression was calculated using the $2^{-\Delta\Delta CT}$ method after normalizing to the expression level of U6 and β-actin.

Western blot assay

Protein from breast cancer cell lines was isolated using RIPA lysis buffer and quantified with a BCA kit (Beyotime, Shanghai, China). Protein was separated via 12% SDS-PAGE and then transferred onto PVDF membranes (EMD Millipore, USA). Subsequently, the membranes were blocked with 5% skimmed milk and treated with primary antibodies overnight at 4°C. Membranes were then probed with HRP-conjugated secondary antibody (1:2,000, ab-6728, Abcam, USA) for 1 h at room temperature. Thereafter, protein bands were visualized by enhanced chemiluminescence (EMD Millipore) and quantified by ImageJ software (version 4.3; National Institutes of Health). The primary antibodies (all from Abcam) were as follows: Anti-E-cadherin (1:1,000, ab1416), anti-vimentin (1:1,000, ab92547), anti-α-smooth muscle actin (SMA, 1:1,000, ab32575), anti-TMEM9B (1:1,000, ab189253) and anti-β-actin (1:1,000, ab8227).

Immunofluorescence assay

Transfected MCF-7 and ZR-75-30 cells were cultured in a six-well plate at a density of 1×10^5 cells/well. After fixation with 4% paraformaldehyde and permeabilization with 0.2% Triton X-100 in PBS, cells were treated with primary

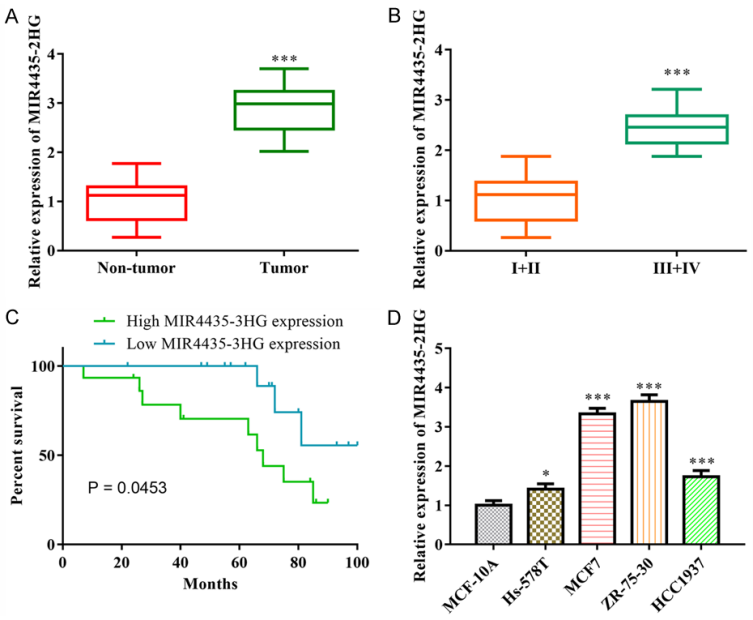

Figure 1. MIR4435-2HG is highly expressed in breast cancer tissues and cell lines. A: The expression of MIR4435-2HG in breast cancer tissues was measured by qRT-PCR, ***P<0.001 *vs.* Non-tumor; B: The expression of MIR4435-2HG in breast cancer tissues at the different stages was measured by qRT-PCR, ***P<0.001 *vs.* I+II; C: Patients with low MIR4435-2HG levels had longer survival times compared with patients with high MIR4435-2HG expression; D: The expression of MIR4435-2HG in breast cancer cell lines was measured by qRT-qPCR, *P<0.05, ***P<0.001 vs. MCF-10A.

antibodies against α-SMA (1:1,000, ab32575) overnight at 4°C. Subsequently, cells were incubated with goat anti-rabbit IgG H&L secondary antibody (1:1,000, ab150077). The nuclei were counter-stained with DAPI. Positive staining was observed under a fluorescence microscope (Zeiss AG, Germany).

Subcellular fractionation analysis

Cytoplasmic and nuclear fractions were extracted from MCF-7 and ZR-75-30 cells using the NE-PER Nuclear and Cytoplasmic Extraction reagent (Thermo Fisher Scientific, Inc., USA). RNA from each fraction was measured by qRT-PCR. GAPDH and U6 were used as internal references for MIR4435-2HG in cytoplasmic and nuclear fractions, respectively.

RNA pull-down analysis

MCF-7 and ZR-75-30 cells were incubated with biotin-labeled miR-22-3p-wild-type (WT) or -mutant (Mut) for 48 h and lysed in the specific buffer. The lysate was incubated with magnetic beads and washed three times with pre-cooled lysis buffer and salt buffer solution. Finally, the bound RNA was purified with TRIzol®. MIR4435-2HG or miR-22-3p enrichment was analyzed using qRT-PCR.

Dual-luciferase reporter assay

The sequences of MIR4435-2HG-WT and TMEM9B-WT and MIR4435-2HG-Mut and TMEM9B-Mut were inserted into the pmirGLO reporter vector (GenScript, Shanghai, China). Subsequently, pmirGLO-MIR-4435-2HG-WT/Mut and pmirGLO-TMEM9B-WT/Mut were treated with miR-22-3p mimic or NC into MCF-7 and ZR-75-30 cells using Lipofectamine 3000 (Invitrogen; Thermo Fisher Scientific, Inc., USA). Luciferase activity was measured using a dual-luciferase reporter assay system (Promega Corporation, USA).

Statistical analysis

GraphPad Prism 6.0 software was used for graphing. SPSS 17.0 software was used for statistical analysis. All data were expressed as mean ± standard deviation ($\bar{x}$ ± sd). Data comparison between groups was performed by analysis of variance. A pairwise comparison between means was performed by one-way ANOVA with Turkey test. Kaplan-Meier curve was used to analyze the relationship between the expression levels of MIR4435-2HG, miR-22-3p, TMEM9B and overall survival of patients with breast cancer. P<0.05 was considered statistically significant.

Results

MIR4435-2HG is highly expressed in breast cancer tissues and cell lines

To investigate the possible role and underlying mechanisms of MIR4435-2HG in breast cancer, the expression of MIR4435-2HG in breast cancer tissues was firstly evaluated by qRT-PCR. The data of **Figure 1A** showed that

MIR4435-2HG was noatbly over-expressed in breast cancer tissues compared with that in non-tumor tissues (P<0.0001). In addition, the expression of MIR4435-2HG in breast cancer patients at different TNM stages was also analyzed. The data of **Figure 1B** revealed that MIR4435-2HG expression was higher in patients at advanced stage III-IV than that in patients at stage I-II (P<0.0001). Moreover, the clinical significance of aberrant MIR4435-2HG expression in the prognosis of patients was investigated. The results of **Figure 1C** indicated that patients with low MIR4435-2HG expression exhibited improved percent survival as compared with patients with high MIR4435-2HG expression (P=0.0453). Furthermore, qRT-PCR was performed to measure the expression of MIR4435-2HG in breast cancer cells. As expected, the data of **Figure 1D** showed that compared with that in MCF-10A cells, the expression of MIR4435-2HG was obviously higher in breast cancer cells, especially in MCF-7 (P<0.0001) and ZR-75-30 (P<0.0001) cells. These data suggested that MIR4435-2HG was up-regulated in breast cancer tissues and cell lines, and might function as an oncogene in the occurrence and development of breast cancer.

Down-regulation of MIR4435-2HG inhibits the viability, proliferation, migration, invasion and EMT of breast cancer cells

To determine the potential role of MIR4435-2HG in breast cancer, MCF-7 and ZR-75-30 cells were transfected with sh-MIR4435-2HG, and the transfection efficiency was detected by the qRT-PCR assay. As shown in **Figure 2A**, the expression of MIR4435-2HG was obviously decreased in MCF-7 (P=0.0001) and ZR-75-30 (P=0.0002) cells transfected with sh-MIR4435-2HG. Then, a CCK-8 assay was used to evaluate the effects of MIR4435-2HG on the viability of MCF-7 and ZR-75-30 cells. The data of **Figure 2B** showed that down-regulation of MIR4435-2HG significantly inhibited the viability of MCF-7 (P=0.0023) and ZR-75-30 (P=0.0112) cells in a time-dependent manner. Besides, a colony formation assay was performed to assess the effects of MIR4435-2HG on the proliferation of MCF-7 and ZR-75-30 cells. The data of **Figure 2C** showed that MIR4435-2HG inhibition significantly suppressed the proliferation of MCF-7 (P=0.0006) and ZR-75-30 (P=0.0006) cells. Moreover, the role of MIR4435-2HG in metastasis of MCF-7 and ZR-75-30 cells was also investigated. The wound healing (MCF-7: P=0.0021; ZR-75-30: P=0.0023) and transwell results showed that down-regulation of MIR4435-2HG significantly blocked migration (MCF-7: P=0.0003; ZR-75-30: P=0.0006) and invasion (MCF-7: P<0.0001; ZR-75-30: P=0.0001) of MCF-7 and ZR-75-30 cells (**Figure 2D**, **2E**). Furthermore, the effects of MIR4435-2HG on the EMT progress of MCF-7 and ZR-75-30 cells were explored. The data of immunofluorescence assay showed that sh-MIR4435-2HG significantly inhibited α-SMA expression (**Figure 2F**). Western blotting was performed to evaluate the effects of MIR4435-2HG on the expression levels of EMT-related proteins, including E-cadherin, vimentin and α-SMA. The data of **Figure 2G** revealed that sh-MIR4435-2HG significantly decreased the protein expression of Vimentin (MCF-7: P=0.0003; ZR-75-30: P=0.0007) and α-SMA (MCF-7: P=0.0002; ZR-75-30: P=0.0008) and increased the level of E-cadherin (MCF-7: P<0.0001; ZR-75-30: P<0.0001) protein in MCF-7 and ZR-75-30 cells. These data suggested that down-regulation of MIR4435-2HG inhibited the viability, proliferation, migration, invasion and EMT of breast cancer cells.

MIR4435-2HG acts as a competing endogenous RNA (ceRNA) via sponging miR-22-3p

To determine the possible mechanisms of MIR4435-2HG in breast cancer, the distribution of MIR4435-2HG was initially investigated by subcellular fraction analysis. As shown in **Figure 3A**, MIR4435-2HG was primarily found in the cytoplasm. In addition, bioinformatics tools were utilized to acquire miRNAs that potentially bound to MIR4435-2HG. As indicated in **Figure 3B**, miR-22-3p was predicted to possess the target domain for MIR4435-2HG. Then miR-22-3p mimic and mimic NC were transfected into MCF-7 (P=0.0042) and ZR-75-30 (P=0.0059) cells, and qRT-PCR was performed to detect transfection efficiency (**Figure 3C**). Dual-luciferase reporter analysis was performed to validate the interaction between MIR4435-2HG and miR-22-3p. As expected, the data of **Figure 3D** showed that exogenous expression of miR-22-3p significantly decreased the luciferase intensity of MCF-7 (P=0.0222) and ZR-75-30 (P=0.0076) cells transfected with MIR4435-2HG-WT. Similarly, RNA pull-down data showed that MIR4435-2HG was highly enriched in MCF-7 (P<0.0001) and ZR-75-30 (P<0.0001) cells with miR-22-3p-WT (**Figure 3E**). Furthermore, the expression of

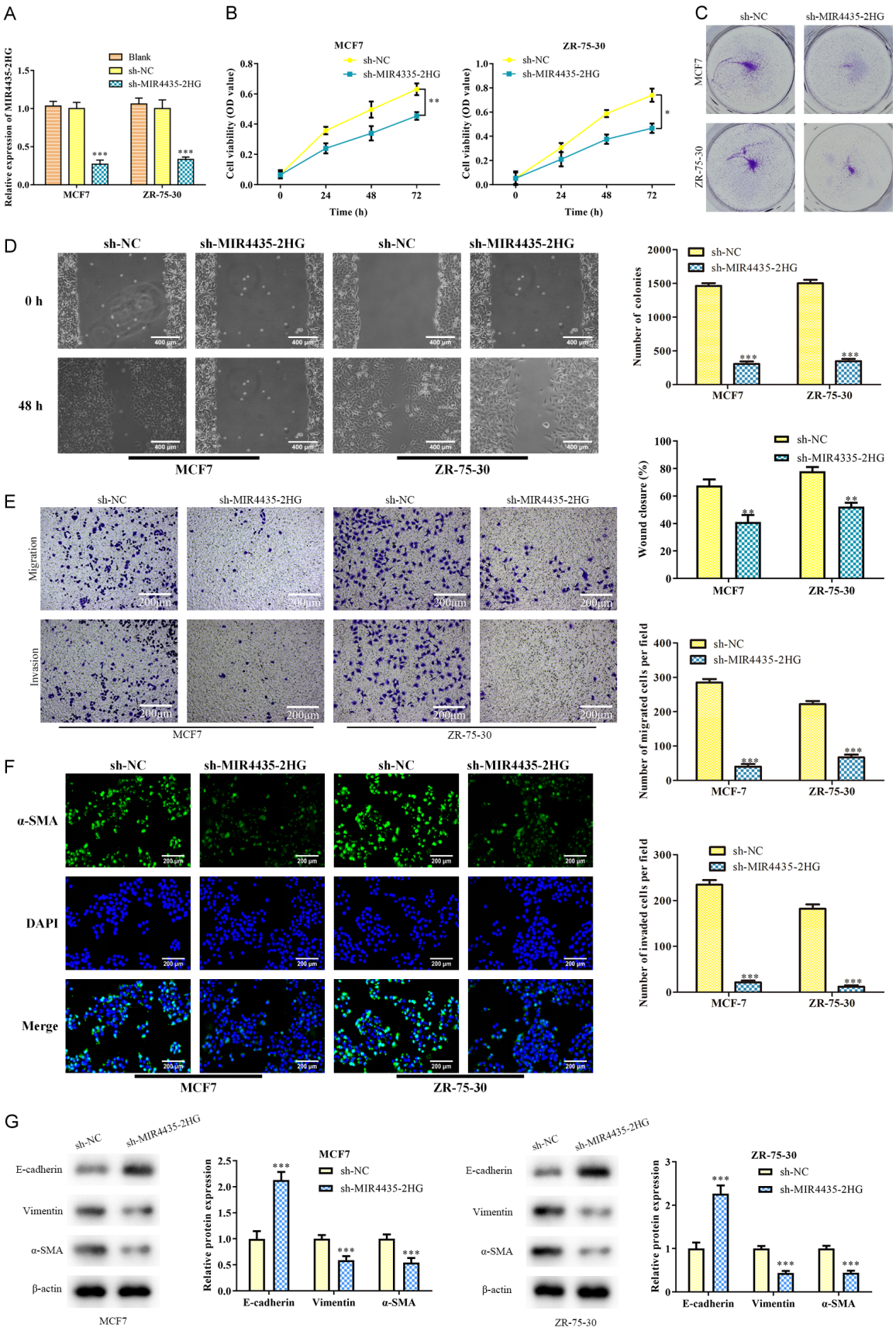
A
Relative expression of MIR4435-2HG
Blank
sh-NC
sh-MIR4435-2HG
MCF7
ZR-75-30
B
MCF7
ZR-75-30
Cell viability (OD value)
Time (h)
C
sh-NC
sh-MIR4435-2HG
D
0 h
48 h
Number of colonies
Wound closure (%)
E
Migration
Invasion
Number of migrated cells per field
Number of invaded cells per field
F
α-SMA
DAPI
Merge
G
E-cadherin
Vimentin
α-SMA
β-actin
Relative protein expression

Figure 2. Down-regulation of MIR4435-2HG inhibits the viability, proliferation, migration, invasion and EMT of breast cancer cells. A: The expression of MIR4435-2HG in MCF-7 and ZR-75-30 cells transfected with sh-MIR4435-2HG was determined by qRT-qPCR; B: The viability of MCF-7 and ZR-75-30 cells transfected with sh-MIR4435-2HG was assessed by CCK-8 assay at the indicated times; C: The proliferation of MCF-7 and ZR-75-30 cells transfected with sh-MIR4435-2HG was assessed by colony formation assay; D: The migration of MCF-7 and ZR-75-30 cells transfected with sh-MIR4435-2HG was determined by wound healing assay (100X); E: The migration and invasion of MCF-7 and ZR-75-30 cells transfected with sh-MIR4435-2HG were determined by transwell migration and invasion assays (100X); F: The protein expression of α-SMA in MCF-7 and ZR-75-30 cells transfected with sh-MIR4435-2HG was assessed by immunofluorescence assay (400X); G: The expression levels of proteins, including E-cadherin, vimentin and α-SMA, in MCF-7 and ZR-75-30 cells transfected with sh-MIR4435-2HG were evaluated by Western blot assay. *P<0.05, **P<0.01, ***P<0.001 *vs.* sh-NC.

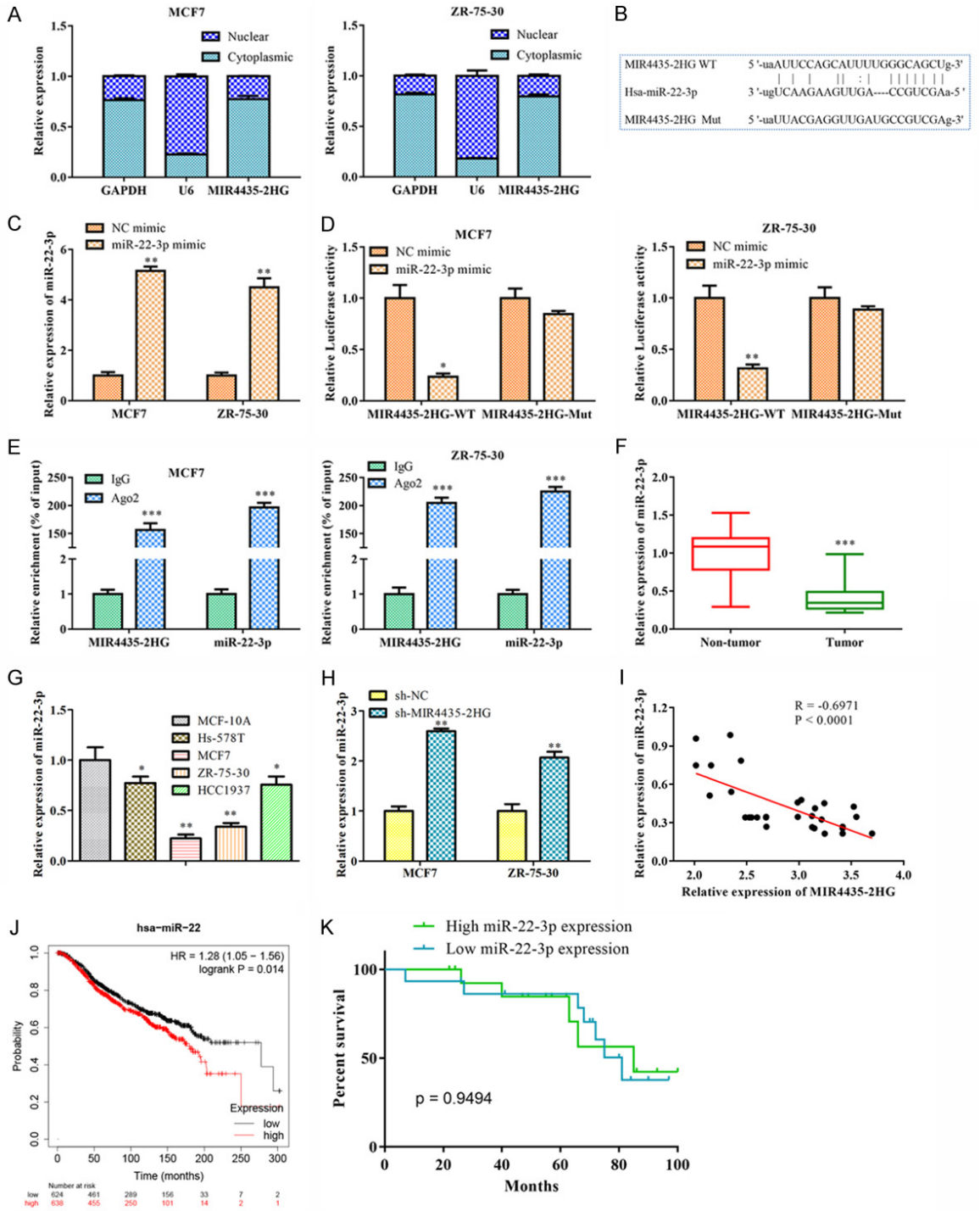

Figure 3. MIR4435-2HG acts as a ceRNA via sponging miR-22-3p. A: The cellular location of MIR4435-2HG was assessed by subcellular fractionation analysis; B: Binding sites between MIR4435-2HG and miR-22-3p; C: The expression of miR-22-3p in MCF-7 and ZR-75-30 cells transfected with miR-22-3p mimic was measured by the qRT-PCR assay; D: The interaction between MIR4435-2HG and miR-22-3p was evaluated by a dual-luciferase reporter assay; C and D: *P<0.05, **P<0.01 *vs.* NC mimic; E: Relative enrichment of MIR4435-2HG and miR-22-3p in MCF-7 and ZR-75-30 cells was measured by RNA pull-down assay, ***P<0.001 *vs.* IgG. F and G: The expression of miR-22-3p in breast cancer tissues (***P<0.001 *vs.* Non-tumor) and cell lines was measured by the qRT-PCR assay (*P<0.05, **P<0.01 *vs.* MCF-10A); H: The expression of miR-22-3p in MCF-7 and ZR-75-30 cells transfected with sh-MIR4435-2HG was assessed by qRT-PCR assay, **P<0.01 *vs.* sh-NC; I: Correlation analysis between MIR4435-2HG and miR-22-3p in breast cancer tissues. J: Influence of miR-22 expression on overall survival rate of breast cancer patients was analyzed by Kaplan-Meier Plotter. K: The survival rate in breast cancer patients with high miR-22-3p expression and low miR-22-3p expression.

miR-22-3p was down-regulated in breast cancer tissues (P<0.0001) and cell lines (MCF-7: P<0.0001; ZR-75-30: P<0.0001) (**Figure 3F**, **3G**) and was significantly up-regulated in MCF-7 (P=0.0029) and ZR-75-30 (P=0.0065) cells transfected with sh-MIR4435-2HG (**Figure 3H**). A negative association (P<0.0001) was also discovered between MIR4435-2HG and miR-22-3p levels in breast cancer tissues (**Figure 3I**). Kaplan-Meier Plotter displayed that high levels of miR-22 expression led to a significant reduction in overall survival (**Figure 3J**, P=0.014). However, our study found no association between miR-22-3p and overall survival (**Figure 3K**, P=0.9494). These data suggested that MIR4435-2HG served as a ceRNA for miR-22-3p in breast cancer.

Up-regulation of miR-22-3p inhibits the viability, proliferation, migration, invasion and EMT of breast cancer cells

CCK-8 assay was performed to evaluate the effects of miR-22-3p on the viability of MCF-7 and ZR-75-30 cells. As shown in **Figure 4A**, miR-22-3p mimic significantly inhibited the viability of MCF-7 (P=0.0016) and ZR-75-30 (P=0.0042) cells in a time-dependent manner. Moreover, a colony formation assay was performed to assess the effects of miR-22-3p on the proliferation of MCF-7 and ZR-75-30 cells. The data in **Figure 4B** showed that up-regulation of miR-22-3p remarkably suppressed the proliferation of MCF-7 (P=0.0057) and ZR-75-30 (P=0.0054) cells. Then the data of wound healing (MCF-7: P=0.0017; ZR-75-30: P=0.0068) and transwell assays showed that miR-22-3p mimic significantly inhibited the migration (MCF-7: P=0.0032; ZR-75-30: P=0.0184) and invasion (MCF-7: P=0.0016; ZR-75-30: P=0.0039) of MCF-7 and ZR-75-30 cells (**Figure 4C**, **4D**). Additionally, a immunofluorescence assay was performed to evaluate the effects of miR-22-3p on the expression of α-SMA. The results showed that miR-22-3p mimic significantly inhibited α-SMA expression (**Figure 4E**). Furthermore, Western blotting was performed to evaluate the effects of miR-22-3p on the expression levels of EMT-related proteins. The data in **Figure 4F** revealed that miR-22-3p mimic significantly decreased the protein expression of Vimentin (MCF-7: P=0.0001; ZR-75-30: P=0.0001) and α-SMA (MCF-7: P=0.0001; ZR-75-30: P<0.0001) and increased the level of E-cadherin (MCF-7: P<0.0001; ZR-75-30: P<0.0001) protein in MCF-7 and ZR-75-30 cells. These data suggested that up-regulation of miR-22-3p inhibited the viability, proliferation, migration, invasion and EMT of breast cancer cells.

TMEM9B acts as a direct target of miR-22-3p

To investigate the downstream targets of miR-22-3p, bioinformatics tools were utilized to acquire mRNAs potentially bound to miR-22-3p. As indicated in **Figure 5A**, TMEM9B was predicted to possess the target domain of miR-22-3p. Dual-luciferase assay (MCF-7: P=0.0066; ZR-75-30: P=0.0289) results further confirmed the target relationship between miR-22-3p and TMEM9B (**Figure 5B**). In addition, qRT-PCR was performed to detect TMEM9B expression in breast cancer tissues and cell lines. As shown in **Figure 5C**, **5D**, TMEM9B was highly expressed in breast cancer tissues (P<0.0001) and cell lines (MCF-7: P<0.0001; ZR-75-30: P=0.0001). Furthermore, qRT-PCR and Western blot assays were performed to evaluate the mRNA and protein levels of TMEM9B in MCF-7 and ZR-75-30 cells transfected with miR-22-3p mimic or NC mimic. The data in **Figure 5E** (MCF-7: P=0.0207; ZR-75-30: P=0.0272), **Figure 5F** (MCF-7: P=0.0017; ZR-75-30: P=0.0022) revealed that the mRNA and protein expression of TMEM9B were significantly dereased in MCF-7 and ZR-75-30 cells transfected with miR-22-3p mimic. Finally, a negative association (P=0.0005) was discovered between miR-22-3p and TMEM9B levels in breast

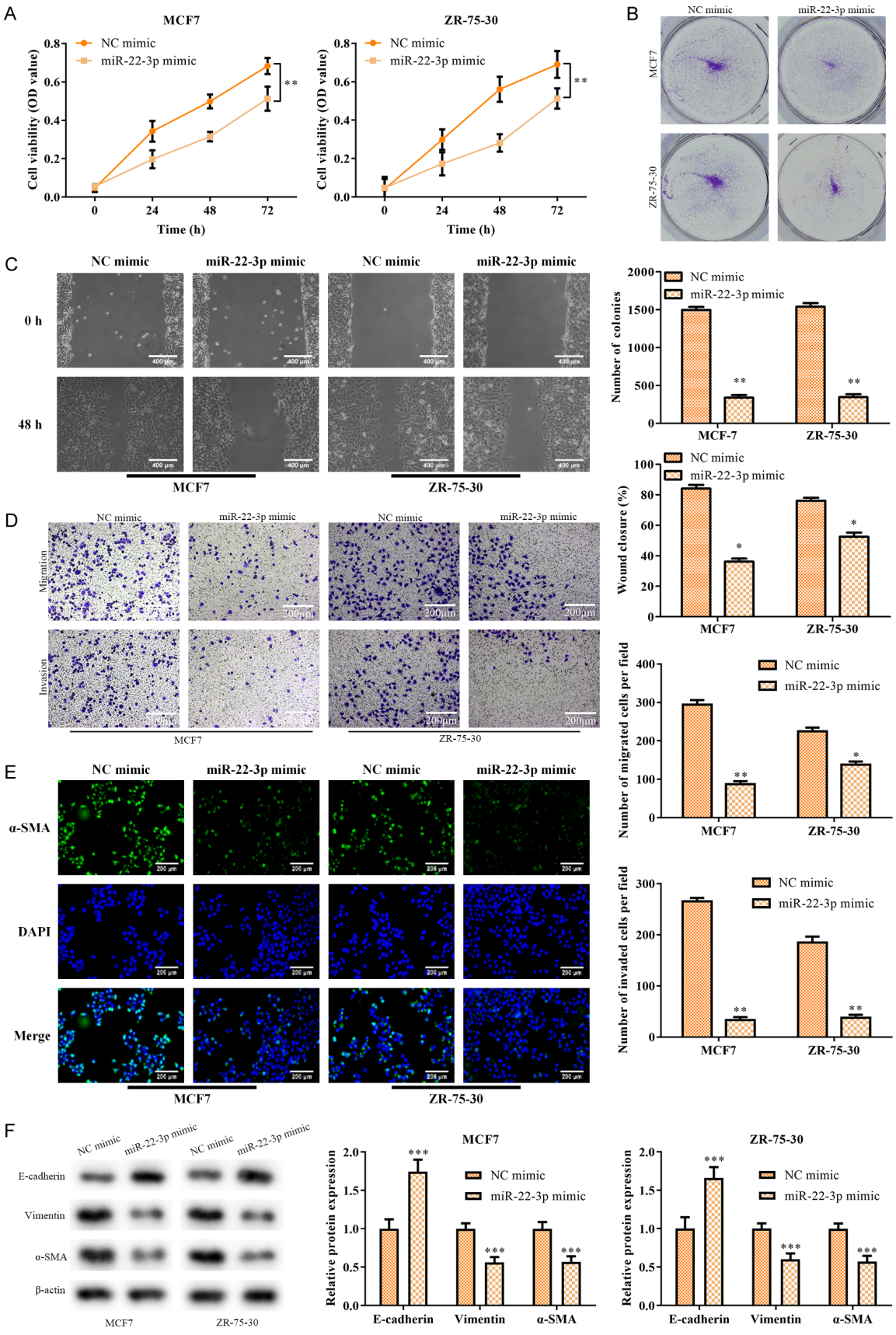
A
MCF7
ZR-75-30
NC mimic
miR-22-3p mimic
Cell viability (OD value)
Time (h)
B
NC mimic
miR-22-3p mimic
MCF7
ZR-75-30
C
0 h
48 h
Number of colonies
MCF-7
D
Migration
Invasion
Wound closure (%)
Number of migrated cells per field
E
α-SMA
DAPI
Merge
Number of invaded cells per field
F
E-cadherin
Vimentin
α-SMA
β-actin
Relative protein expression

Figure 4. Up-regulation of miR-22-3p inhibits the viability, proliferation, migration, invasion and EMT of breast cancer cells. A: The viability of MCF-7 and ZR-75-30 cells transfected with miR-22-3p mimic was assessed by CCK-8 assay at the indicated times; B: The proliferation of MCF-7 and ZR-75-30 cells transfected with miR-22-3p mimic was assessed by colony formation assay; C: The migration of MCF-7 and ZR-75-30 cells transfected with miR-22-3p mimic was determined by wound healing assay (100X); D: The migration and invasion of MCF-7 and ZR-75-30 cells transfected with miR-22-3p mimic were determined by transwell migration and invasion assays (100X); E: The protein expression of α-SMA in MCF-7 and ZR-75-30 cells transfected with miR-22-3p mimic was assessed by immunofluorescence assay (400X); F: The expression levels of proteins, including E-cadherin, vimentin and α-SMA, in MCF-7 and ZR-75-30 cells transfected with miR-22-3p mimic were evaluated by Western blot assay. Compared with NC mimic, *P<0.05, **P<0.01, ***P<0.001.

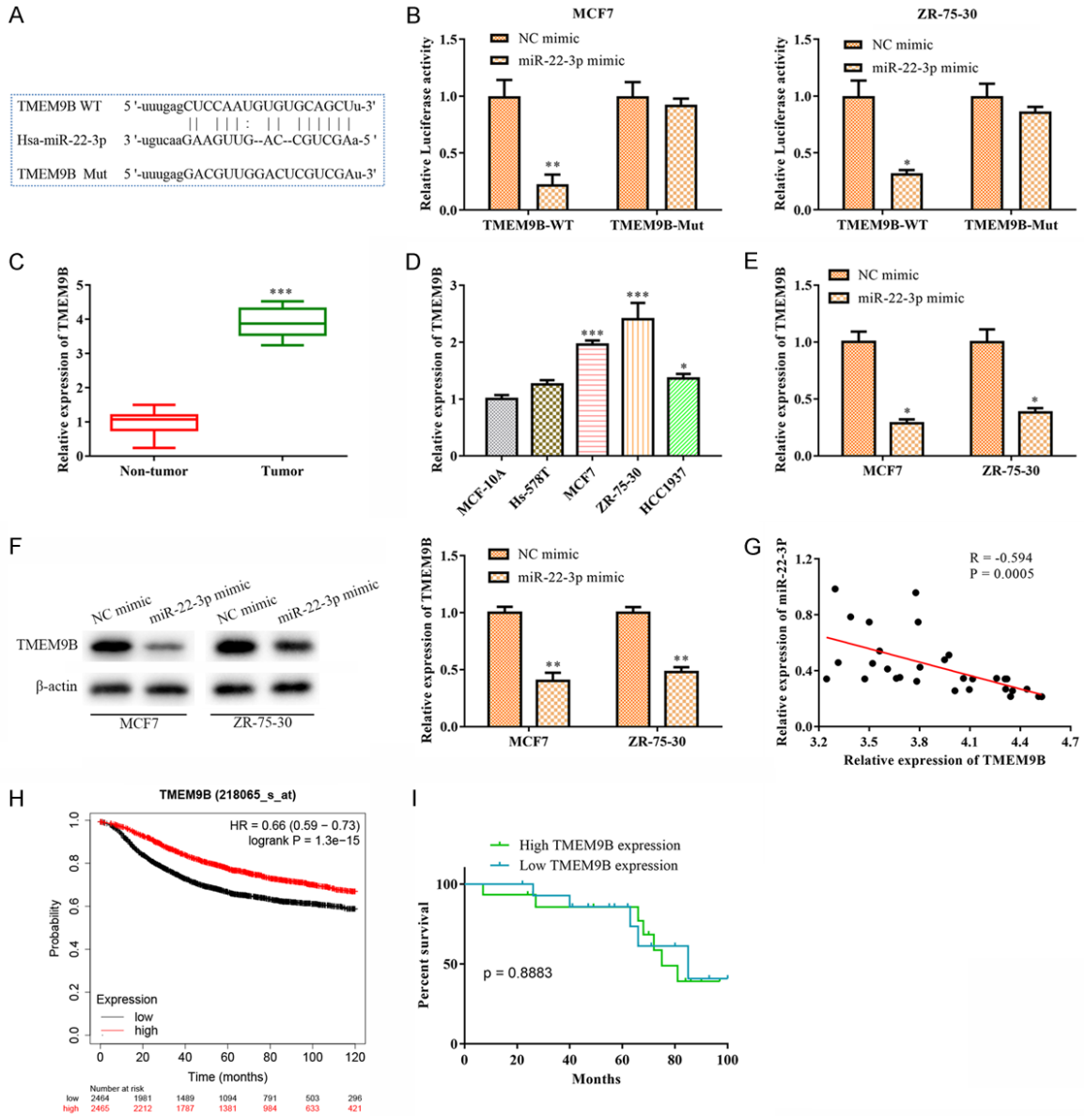

Figure 5. TMEM9B is a direct target gene of miR-22-3p and is negatively associated with miR-22-3p. A: Binding sites between miR-22-3p and TMEM9B; B: The interaction between miR-22-3p and TMEM9B was evaluated by a dual-luciferase reporter assay; C and D: The expression of TMEM9B in breast cancer tissues (**P<0.01 *vs.* Non-tumor) and cell lines was detected by the qRT-PCR assay (*P<0.05, **P<0.001 *vs.* MCF-10A); E and F: The mRNA and protein levels of TMEM9B in MCF-7 and ZR-75-30 cells transfected with miR-22-3p mimic were assessed by qRT-PCR and Western blot assays; G: Correlation analysis between miR-22-3p and TMEM9B in breast cancer tissues. H: Influence of TMEM9B expression on overall survival rate of breast cancer patients was analyzed by Kaplan-Meier Plotter. I: The survival rate in breast cancer patients with high TMEM9B expression and low TMEM9B expression. B, E and F: *P<0.05, **P<0.01 *vs.* NC mimic.

cancer tissues (**Figure 5G**). Kaplan-Meier Plotter indicated that low levels of TMEM9B expression led to a significant reduction in overall survival (**Figure 5H**, P<0.0001). However, there was no association between TMEM9B expression and overall survival in our study (**Figure 5I**, P=0.8883). These data suggested that TMEM9B was a direct target of miR-22-3p and was negatively associated with miR-22-3p in breast cancer.

MIR4435-2HG regulates the viability, proliferation, migration, invasion and EMT of breast cancer cells by modulating the miR-22-3p/TMEM9B axis

To further determine whether MIR4435-2HG exhibited its role by regulating the miR-22-3p/TMEM9B axis, a series of rescue assays were performed. As shown in **Figure 6A**, **6B**, MIR4435-2HG knockdown inhibited the viability (P=0.0013) and proliferation (P<0.0001) of MCF-7 cells. However, the miR-22-3p inhibitor promoted MCF-7 cell viability (P=0.0035) and proliferation (P=0.0002), while TMEM9B2 inhibition exhibited inhibitory effects on the viability (P=0.0375) and proliferation (P=0.0094) of MCF-7 cells. Moreover, results of wound healing and transwell assays indicated that MIR4435-2HG knockdown inhibited the migration (**Figure 6C**: P=0.0001, **Figure 6D**: P<0.0001) and invasion of MCF-7 cells (P<0.0001). However, miR-22-3p inhibitor promoted MCF-7 cell migration (**Figure 6C**: P=0.0009, **Figure 6D**: P<0.0001) and invasion (P=0.0001), while TMEM9B2 inhibition exhibited suppressive effects on the migration (**Figure 6C**: P=0.0036, **Figure 6D**: P<0.0001) and invasion (P=0.0039) of MCF-7 cells. Data from immunofluorescence and Western blot assays illustrated that MIR4435-2HG knockdown inhibited the EMT progression of MCF-7 cells (**Figure 6E**, **6F**). However, miR-22-3p inhibitor promoted MCF-7 cell EMT progression, while TMEM9B2 inhibition exhibited inhibitory effects on EMT progression of MCF-7 cells. These data suggested MIR4435-2HG exerted its role by modulating the miR-22-3p/TMEM9B axis.

Discussion

A large number of studies have confirmed that abnormal expression of MIR4435-2HG plays an essential role in multiple tumors, including gastric cancer, prostate carcinoma and oral squamous cell carcinoma [18-21]. In this study, MIR4435-2HG was clearly up-regulated in breast cancer tissues and cell lines. In addition, breast cancer patients with low MIR4435-2HG expression exhibited improved survival rate compared with those with high MIR4435-2HG expression, which is consistent with previous studies. Functionally, our data showed that down-regulation of MIR4435-2HG notably inhibited the viability, proliferation, migration, invasion and EMT progress of breast cancer cells. Similarly, MIR4435-2HG exhibited its role in promoting the proliferation and metastasis of colorectal cancer and ovarian cancer [22-24]. These data suggested that MIR4435-2HG might act as an oncogene in the occurrence and progression of breast cancer.

LncRNAs affect the occurrence and development of tumors via post-transcriptional regulation [25]. Multiple lncRNAs may regulate gene expression, thus reducing the number of available miRNAs in cells [26]. Therefore, lncRNAs act as competing ceRNAs to modulate the expression of the target genes via sponging miRNAs [27]. In neuroglioma, MIR4435-2HG promotes tumor progression by exerting the ceRNA function of miR-125a-5p [28]. Moreover, MIR4435-2HG acted as a ceRNA of miR-138-5p in gastric carcinoma [29]. In this study, the data indicated that miR-22-3p was a direct target of MIR4435-2HG, which is consistent with the results of Shen *et al.* [30]. Previous studies have illustrated that miR-22-3p exerted essential effects on the development of many tumors, including bladder cancer, gastric cancer and lung cancer [31-33]. The data showed that the level of miR-22-3p was dramatically reduced in breast cancer tissues and cell lines, and was inversely correlated with MIR4435-2HG expression in breast cancer tissues. Moreover, up-regulation of miR-22-3p suppressed the viability, proliferation, migration, invasion and EMT progress of breast cancer cells. These results indicated that miR-22-3p acted as a tumor suppressor in breast cancer.

MiRNAs act as tumor suppressors through the restraint of their target genes to participate in breast cancer progression [34]. Fan *et al.* confirmed that miR-22-3p blocked tumor progression via targeting PLAGL2 in breast cancer [35]. In this study, TMEM9B was confirmed as a target of miR-22-3p. TMEM9B, as a glycosylated protein located on the lysosomal membrane, has been previously discovered as an NF-κB inducer in large-scale cDNA over-expres-

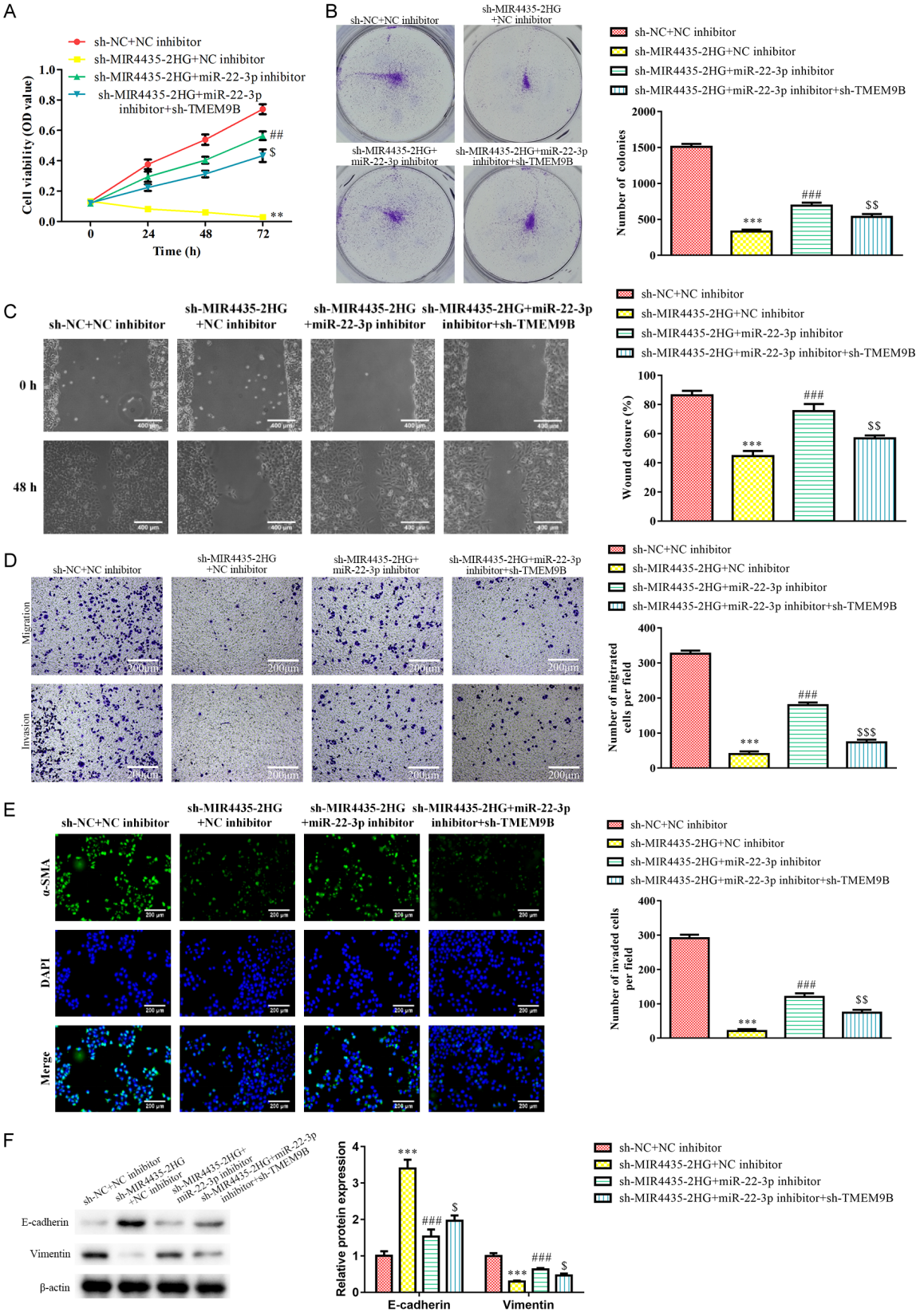

Figure 6. MIR4435-2HG regulates the viability, proliferation, migration, invasion and EMT of breast cancer cells by modulating the miR-22-3p/TMEM9B axis. A: The viability of MCF-7 and ZR-75-30 cells after transfection was assessed by CCK-8 assay at the indicated times; B: The proliferation of MCF-7 and ZR-75-30 cells after transfection

was assessed by colony formation assay; C: The migration of MCF-7 and ZR-75-30 cells after transfection was determined by wound healing assay (100X); D: The migration and invasion of MCF-7 and ZR-75-30 cells after transfection were determined by transwell migration and invasion assays (100X); E: The protein expression of α-SMA in MCF-7 and ZR-75-30 cells after transfection was assessed by immunofluorescence assay (400X); F: The expression levels of proteins, including E-cadherin, vimentin and α-SMA, in MCF-7 and ZR-75-30 cells after transfection were evaluated by Western blot assay. **P<0.01, ***P<0.001 *vs.* sh-NC+NC inhibitor; $^{\#\#}$P<0.01, $^{\#\#\#}$P<0.001 *vs.* sh-MIR4435-2HG+NC inhibitor; $^{\$}$P<0.05, $^{\$\$}$P<0.01, $^{\$\$\$}$P<0.001, *vs.* sh-MIR4435-2HG+miR-22-3p inhibitor.

sion screens [36]. Furthermore, TMEM9B is a key component of inflammatory signaling pathways [37]. A remarkable negative correlation between the expression levels of TMEM9B and miR-22-3p in breast cancer tissues was found in this study. TMEM9B was a direct target of miR-22-3p in breast cancer cells, which indicated that the ceRNA system existed among MIR4435-2HG, miR-22-3p and TMEM9B in breast cancer. Next, our data presented that the effects of MIR4435-2HG knockdown reduced TMEM9B expression level by the promotion of miR-22-3p. TMEM9B inhibition partly restored the effects of the miR-22-3p inhibitor on the viability, proliferation, migration, invasion and EMT progression of breast cancer cells transfected with sh-MIR4435-2HG. The small number of patients is a limitation of this paper, and we will increase the number of patients in later research. In addition, the relationships between other miRNAs targeted by MIR4435-2HG and other genes targeted by miR-22-3p also need to be further studied.

To conclude, MIR4435-2HG was regarded as a vital mediator of cell growth and metastasis in breast cancer. MIR4435-2HG was obviously up-regulated in breast cancer tissues and cell lines, and MIR4435-2HG knockdown blocked breast cancer progression by acting as a ceRNA to down-regulate TMEM9B through competitively binding to miR-22-3p. These results indicated that MIR4435-2HG/miR-22-3p/TMEM9B axis might be a potential therapeutic basis for the treatment of breast cancer.

Acknowledgements

This work was supported by the Nantong Municipal Science and Technology Plan (MSZ-19210).

Disclosure of conflict of interest

None.

Address correspondence to: Haijun Mei, Department of General Surgery, Affiliated Hospital of Nantong University, No.20 Xisi Road, Chongchuan District, Nantong 226001, Jiangsu Province, China. Tel: +86-0513-85052565; Fax: +86-0513-8505-2565; E-mail: 15996692626@163.com

References

[1] Fahad Ullah M. Breast cancer: current perspectives on the disease status. Adv Exp Med Biol 2019; 1152: 51-64.

[2] Monticciolo DL, Newell MS, Moy L, Niell B, Monsees B and Sickles EA. Breast cancer screening in women at higher-than-average risk: recommendations from the ACR. J Am Coll Radiol 2018; 15: 408-414.

[3] Shamsi M and PirayeshIslamian J. Breast cancer: early diagnosis and effective treatment by drug delivery tracing. Nucl Med Rev Cent East Eur 2017; 20: 45-48.

[4] He Y, Liu H, Chen Q, Shao Y and Luo S. Relationships between SNPs and prognosis of breast cancer and pathogenic mechanism. Mol Genet Genomic Med 2019; 7: e871.

[5] Ghoncheh M, Pournamdar Z and Salehiniya H. Incidence and mortality and epidemiology of breast cancer in the world. Asian Pac J Cancer Prev 2016; 17: 43-46.

[6] Li YL, Qin YC, Tang LY, Liao YH, Zhang W, Xie XM, Liu Q, Lin Y and Ren ZF. Patient and care delays of breast cancer in China. Cancer Res Treat 2019; 51: 1098-1106.

[7] Liang Y, Zhang H, Song X and Yang Q. Metastatic heterogeneity of breast cancer: molecular mechanism and potential therapeutic targets. Semin Cancer Biol 2020; 60: 14-27.

[8] Jafari SH, Saadatpour Z, Salmaninejad A, Momeni F, Mokhtari M, Nahand JS, Rahmati M, Mirzaei H and Kianmehr M. Breast cancer diagnosis: imaging techniques and biochemical markers. J Cell Physiol 2018; 233: 5200-5213.

[9] Soudyab M, Iranpour M and Ghafouri-Fard S. The role of long non-coding rnas in breast cancer. Arch Iran Med 2016; 19: 508-517.

[10] Yang F, Lyu S, Dong S, Liu Y, Zhang X and Wang O. Expression profile analysis of long noncoding RNA in HER-2-enriched subtype breast cancer by next-generation sequencing and bioinformatics. Onco Targets Ther 2016; 9: 761-772.

[11] Shen X, Xie B, Ma Z, Yu W, Wang W, Xu D, Yan X, Chen B, Yu L, Li J, Chen X, Ding K and Cao F. Identification of novel long non-coding RNAs

in triple-negative breast cancer. Oncotarget 2015; 6: 21730-21739.
[12] Yang F, Lv SX, Lv L, Liu YH, Dong SY, Yao ZH, Dai XX, Zhang XH and Wang OC. Identification of lncRNA FAM83H-AS1 as a novel prognostic marker in luminal subtype breast cancer. Onco Targets Ther 2016; 9: 7039-7045.
[13] Ye N, Wang B, Quan ZF, Cao SJ, Wen XT, Huang Y, Huang XB, Wu R, Ma XP and Yan QG. Functional roles of long non-coding rna in human breast cancer. Asian Pac J Cancer Prev 2014; 15: 5993-5997.
[14] Liu B, Pan CF, Ma T, Wang J, Yao GL, Wei K and Chen YJ. Long non-coding RNA AK001796 contributes to cisplatin resistance of non-small cell lung cancer. Mol Med Rep 2017; 16: 4107-4112.
[15] Ouyang W, Ren L, Liu G, Chi X and Wei H. LncRNA MIR4435-2HG predicts poor prognosis in patients with colorectal cancer. PeerJ 2019; 7: e6683.
[16] Kong Q, Liang C, Jin Y, Pan Y, Tong D, Kong Q and Zhou J. The lncRNA MIR4435-2HG is upregulated in hepatocellular carcinoma and promotes cancer cell proliferation by upregulating miRNA-487a. Cell Mol Biol Lett 2019; 24: 26.
[17] Zhu L, Wang A, Gao M, Duan X and Li Z. LncRNA MIR4435-2HG triggers ovarian cancer progression by regulating miR-128-3p/CKD14 axis. Cancer Cell Int 2020; 20: 145.
[18] Wang H, Wu M, Lu Y, He K, Cai X, Yu X, Lu J and Teng L. LncRNA MIR4435-2HG targets desmoplakin and promotes growth and metastasis of gastric cancer by activating Wnt/β-catenin signaling. Aging (Albany NY) 2019; 11: 6657-6673.
[19] Zhang H, Meng H, Huang X, Tong W, Liang X, Li J, Zhang C and Chen M. lncRNA MIR4435-2HG promotes cancer cell migration and invasion in prostate carcinoma by upregulating TGF-β1. Oncol Lett 2019; 18: 4016-4021.
[20] Shen H, Sun B, Yang Y, Cai X, Bi L, Deng L and Zhang L. MIR4435-2HG regulates cancer cell behaviors in oral squamous cell carcinoma cell growth by upregulating TGF-β1. Odontology 2020; 108: 553-559.
[21] Yang M, He X, Huang X, Wang J, He Y and Wei L. LncRNA MIR4435-2HG-mediated upregulation of TGF-β1 promotes migration and proliferation of nonsmall cell lung cancer cells. Environ Toxicol 2020; 35: 582-590.
[22] Dong X, Yang Z, Yang H, Li D and Qiu X. Long non-coding RNA MIR4435-2HG promotes colorectal cancer proliferation and metastasis through miR-206/YAP1 axis. Front Oncol 2020; 10: 160.
[23] Liu S, Qiao Z, Ma Q, Liu X and Ma X. LncRNA CYTOR and MIR4435-2HG in ovarian cancer and its relationship with clinicopathological features. Panminerva Med 2019; 64: 119-120.
[24] Wang R, Liu L, Jiao J and Gao D. Knockdown of MIR4435-2HG suppresses the proliferation, migration and invasion of cervical cancer cells via regulating the miR-128-3p/MSI2 axis in vitro. Cancer Manag Res 2020; 12: 8745-8756.
[25] Dykes IM and Emanueli C. Transcriptional and post-transcriptional gene regulation by long non-coding RNA. Genomics Proteomics Bioinformatics 2017; 15: 177-186.
[26] Salmena L, Poliseno L, Tay Y, Kats L and Pandolfi PP. A ceRNA hypothesis: the rosetta stone of a hidden RNA language? Cell 2011; 146: 353-358.
[27] Chan JJ and Tay Y. Noncoding RNA: RNA regulatory networks in cancer. Int J Mol Sci 2018; 19: 1310.
[28] Shen W, Zhang J, Pan Y and Jin Y. LncRNA MIR4435-2HG functions as a ceRNA against miR-125a-5p and promotes neuroglioma development by upregulating TAZ. J Clin Lab Anal 2021; 35: e24066.
[29] Gao L, Li W, Liu Y, Zhang C, Gao W and Wang L. Inhibition of MIR4435-2HG on invasion, migration, and EMT of gastric carcinoma cells by mediating MiR-138-5p/Sox4 axis. Front Oncol 2021; 11: 661288.
[30] Shen X, Ding Y, Lu F, Yuan H and Luan W. Long noncoding RNA MIR4435-2HG promotes hepatocellular carcinoma proliferation and metastasis through the miR-22-3p/YWHAZ axis. Am J Transl Res 2020; 12: 6381-6394.
[31] Tian Y, Guan Y, Su Y, Yang T and Yu H. TRPM2-AS promotes bladder cancer by targeting miR-22-3p and regulating GINS2 mRNA expression. Onco Targets Ther 2021; 14: 1219-1237.
[32] He W, Zhang Y and Xia S. LncRNA NNT-AS1 promotes non-small cell lung cancer progression through regulating miR-22-3p/YAP1 axis. Thorac Cancer 2020; 11: 549-560.
[33] Gan L, Lv L and Liao S. Long non-coding RNA H19 regulates cell growth and metastasis via the miR-22-3p/Snail1 axis in gastric cancer. Int J Oncol 2019; 54: 2157-2168.
[34] Loh HY, Norman BP, Lai KS, Rahman N, Alitheen NBM and Osman MA. The regulatory role of MicroRNAs in breast cancer. Int J Mol Sci 2019; 20: 4940.
[35] Fan T, Wang C, Li X, Yang H, Zhou J and Song Y. MiR-22-3p suppresses cell migration and invasion by targeting PLAGL2 in breast cancer. J Coll Physicians Surg Pak 2021; 31: 937-940.
[36] Rovillain E, Mansfield L, Lord CJ, Ashworth A and Jat PS. An RNA interference screen for identifying downstream effectors of the p53 and pRB tumour suppressor pathways involved in senescence. BMC Genomics 2011; 12: 355.
[37] Dodeller F, Gottar M, Huesken D, Iourgenko V and Cenni B. The lysosomal transmembrane protein 9B regulates the activity of inflammatory signaling pathways. J Biol Chem 2008; 283: 21487-21494.